First- and Last-Passage Algorithms in Diffusion Monte Carlo

James A. Given[1], Chi-Ok Hwang[2], and Michael Mascagni[3]

[1] Angle Inc., 7406 Alban Station Court, Suite A112, Springfield, VA 22150 **USA**,
E-mail: given@angleinc.com
[2] Department of Computer Science, Florida State University,
203 Love Building, Tallahassee, FL 32306-4530, **USA**,
E-mail: chwang@csit.fsu.edu
URL: http://www.cs.fsu.edu/~chwang
[3] Department of Computer Science, Florida State University,
203 Love Building, Tallahassee, FL 32306-4530, **USA**,
E-mail: mascagni@cs.fsu.edu
URL: http://www.cs.fsu.edu/~mascagni

Abstract. This paper provides a review of a new method of addressing problems in diffusion Monte Carlo: the Green's function first-passage method (GFFP). In particular, we address four new strands of thought and their interaction with the GFFP method: the use of angle-averaging methods to reduce vector or tensor Laplace equations to scalar Laplace equations; the use of the simulation-tabulation (ST) method to dramatically expand the range of the GFFP method; the use of the Feynman-Kac formula, combined with GFFP to actually perform path integrals, one patch at a time; and the development of last-passage diffusion methods; these drastically improve the efficiency of diffusion Monte Carlo methods. All of these techniques are described in detail, with specific examples.

1 Introduction

Many researchers have used diffusion Monte Carlo methods to calculate the bulk properties of porous and composite media. Basic examples of such properties include: the electrical or thermal conductivity [1–4] or shear modulus of structural composites; the permeability of porous media [5]; the electrostatic contribution to the free energy of a bio-molecule in solution; and the mutual capacitance matrix describing interaction of micro-components in a transistor matrix on a microchip. Porous and composite media have basic geometric similarities: they involve samples of bulk matter that are composed of small patches of two (or more) pure phases. Both the bulk material properties of each pure phase and the statistics of the mixture, *i.e.*, its correlation functions, are assumed to be known. This information can be used to determine the bulk properties of the multi-phase medium.

The two classes of problems also share a deeper, mathematical foundation: they involve the solution of elliptic or parabolic partial differential equations

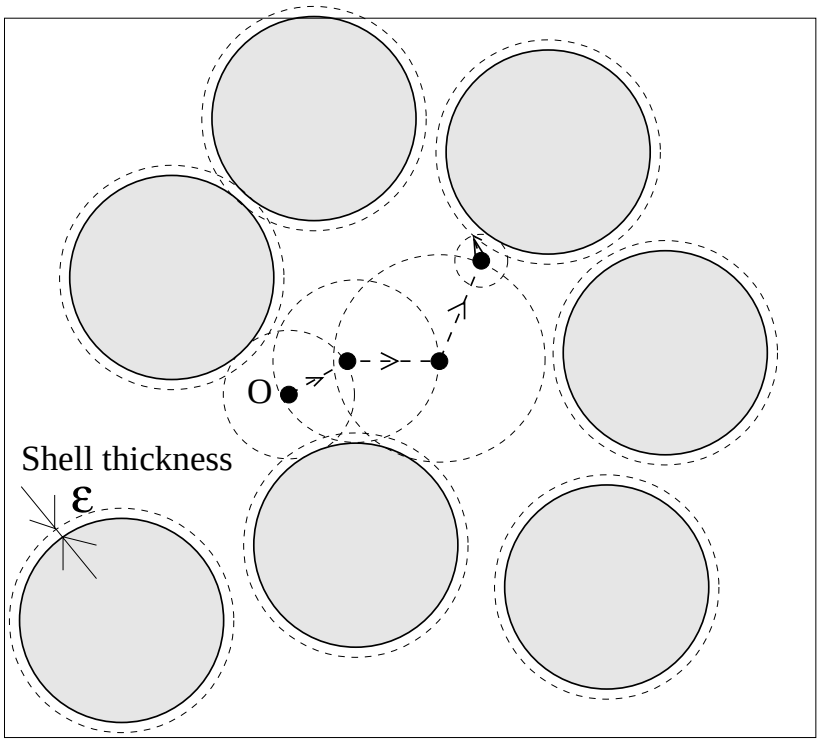

Fig. 1. A two-dimensional schematic representation of a Brownian trajectory using WOS algorithm. If the diffusing particle reaches the ϵ-layer, it is taken to be absorbed.

in domains that contain a large amount of surface area, *i.e.*, interface area, at which boundary conditions must be imposed. Standard finite-element or boundary element methods require long computation times in these cases, especially when high accuracy is required. Considerable cost is associated with discretizing complicated interfaces. These problems can be efficiently solved by diffusion Monte Carlo techniques: the problem in question is modeled as an (in general) anisotropic, biased diffusion problem. Many methods, at this step, employ a discrete representation in either space or time of the underlying Brownian motion; as we show, the availability of Green's functions for the continuum problem makes this unnecessary.

Here we describe a new approach to such problems, the Green's function first-passage (GFFP) method. It is a synthesis of advances developed by this group, and those developed elsewhere; of ideas from pure mathematics and those from applied mathematics. In particular, the GFFP method involves:

• Using the angle-averaging method to reduce problems based on vector or tensor Laplace equations to problems based on scalar Laplace equations, *i.e.*, on biased diffusion equations.

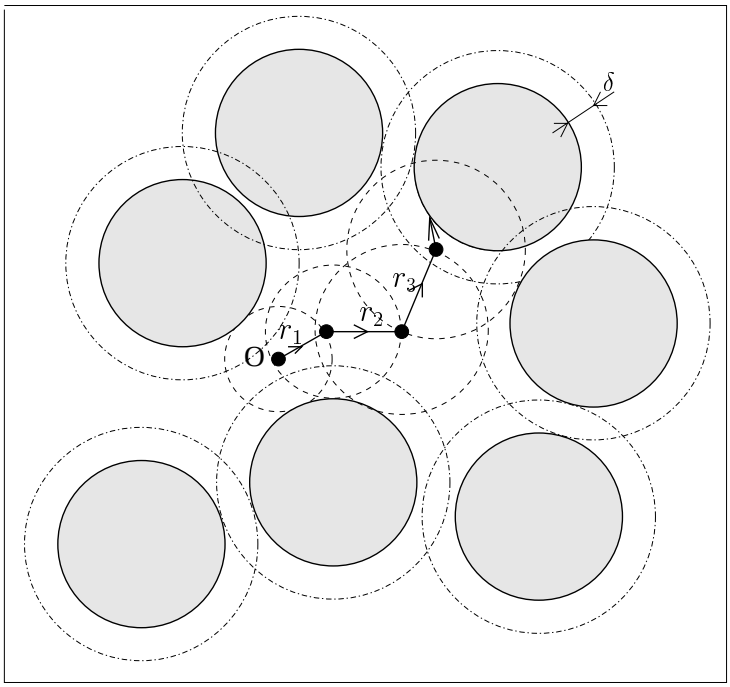

Fig. 2. A two-dimensional schematic representation of a Brownian trajectory using both the WOS algorithm (r_1 to r_3) and the GFFP algorithm (the final step). The solid circles are FP boundaries and absorbing. We use a δ-boundary layer as a criterion such that WOS is used outside the δ-boundary layer and GFFP in the δ-boundary layer,

• Defining the solution to the problem in question in terms of sources and sinks of diffusing particles. For example, an electrostatic problem is cast as an effort to calculate the surface charge density on all interfaces. Once this is done, voltages, or other quantities defined as weighted averages over the surface charge density, can be calculated efficiently by using, *e. g.*, the fast multi-pole method.

• Describing the calculation to be conducted as the simulation of a large number of Brownian trajectories. These may either begin at charge sources or sinks, as in last-passage algorithms [6], or terminate at them, as in first-passage algorithms [7].

• Modeling the interface between phases as locally smooth, *i.e.*, as locally consisting of patches that are flat, spherical, cylindrical, or otherwise understood in terms of their Laplacian Green's function.

• Modeling the free diffusion of particles in such an environment by using a first-passage (FP) strategy. We divide the trajectory of a Brownian particle into a series of jumps, each one taking the Brownian particle from the center

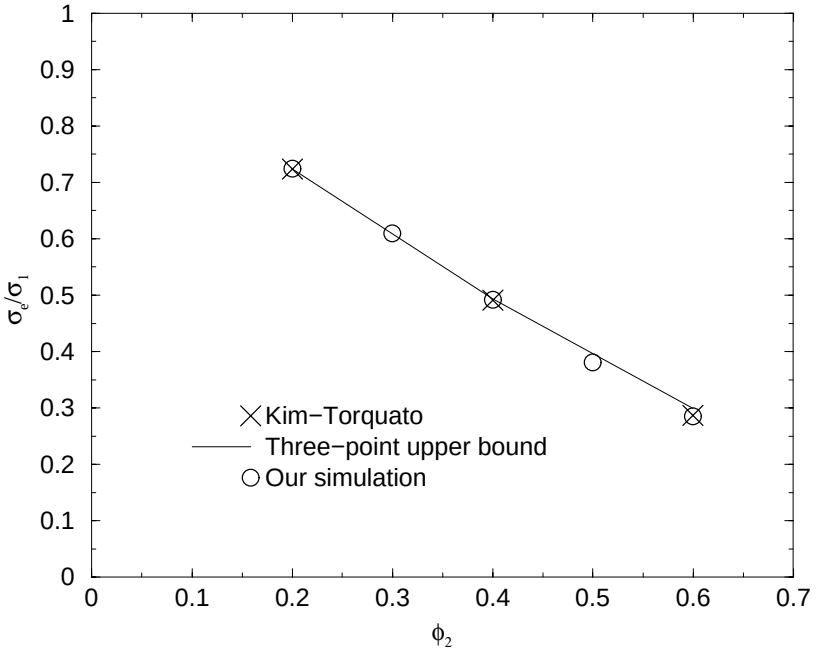

Fig. 3. Scaled effective conductivity σ_e/σ_1 of equilibrium distributions of nonoverlapping insulating spheres in a matrix of conductivity σ_1 with $\epsilon = 0$ and $\delta = 0.1a$.

of a FP volume to a point on the FP surface. FP surfaces far from absorbing boundaries are spheres (this approach replicates the "walk on spheres" (WOS) algorithm [8–10]. see Fig 1). But near absorbing boundaries, FP surfaces can be more complicated. They can include portions of an absorbing boundary. Acceptable FP surfaces, at this stage of analysis, are those for which a quasi-analytic Green's function exists for the corresponding Dirichlet problem. Such Green's functions (actually the normalized distribution functions corresponding to them) can be tabulated for each set of values of the dimensionless geometric parameters they depend on. This tabulation can then be closely approximated by a spline or other interpolatory fit, which in turn allows rapid and accurate sampling of the FP position during a Monte Carlo simulation (see Fig 2). It has been shown that this method is substantially more efficient computationally in applications for which high accuracy is required [11].

As an example, in Fig. 3 we show the effective conductivity of a two-phase medium, consisting of an ensemble of nonoverlapping, insulating spherical inclusions dispersed randomly in a matrix phase of finite conductivity σ_1. We compare the CPU time of the GFFP algorithm with that of the WOS algorithm in Figs. 4 and 5. In the WOS algorithm, CPU time depends on the ϵ-shell thickness while in the GFFP algorithm it depends on δ-boundary layer. The ϵ-shell around the target is used to establish convergence in the WOS method, such that any Brow-

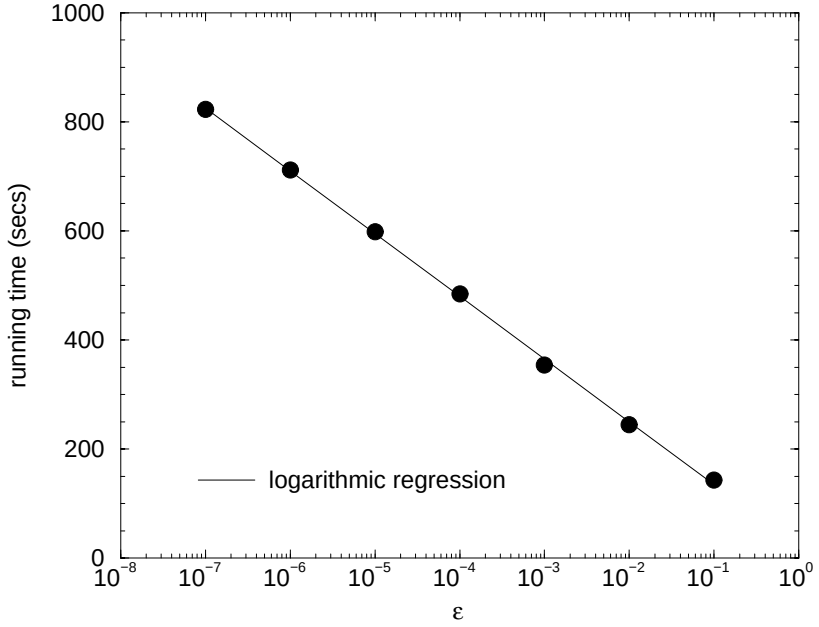

Fig. 4. CPU time required to calculate the effective conductivity of a system of non-overlapping, insulating spherical inclusions dispersed randomly in a conducting matrix with sink volume fraction $\phi_2 = 0.2$. Here, we used the WOS method with mean diffusion path length $X^2/a^2 = 100$. Times here were measured on a 500 MHz Pentium III work station running Linux over 10^4 Brownian trajectories. The simulations show the expected relation for WOS: CPU time proportional to $\ln(\epsilon)$).

nian particle inside it is taken to be absorbed. Also, we use a δ-boundary layer as a criterion such that WOS is used outside the δ-boundary layer and GFFP in the δ-boundary layer, because GFFP is more efficient as the Brownian particle approaches the boundary. Here, $\epsilon = 10^{-1}$ in the WOS method approximately corresponds to the optimal case of GFFP.

Algorithms developed from the GFFP method already provide the most efficient algorithms known for certain important classes of problems, including the electrostatic capacitance of an arbitrary object. For example, the most accurate value for the capacitance of the unit cube is $C = 0.660675(5)$. For comparison, the most accurate value for this quantity yet obtained from boundary element methods is uncertain in the third digit, due to the logarithmic convergence involved in applying these methods to surfaces with edges and corners.

But much more is possible, using the diffusion Monte Carlo methodology. We combine it with:

• optimal applied mathematics methods; these include the simulation-tabulation (ST) method [12], and the efficient generation of quasi-random numbers;

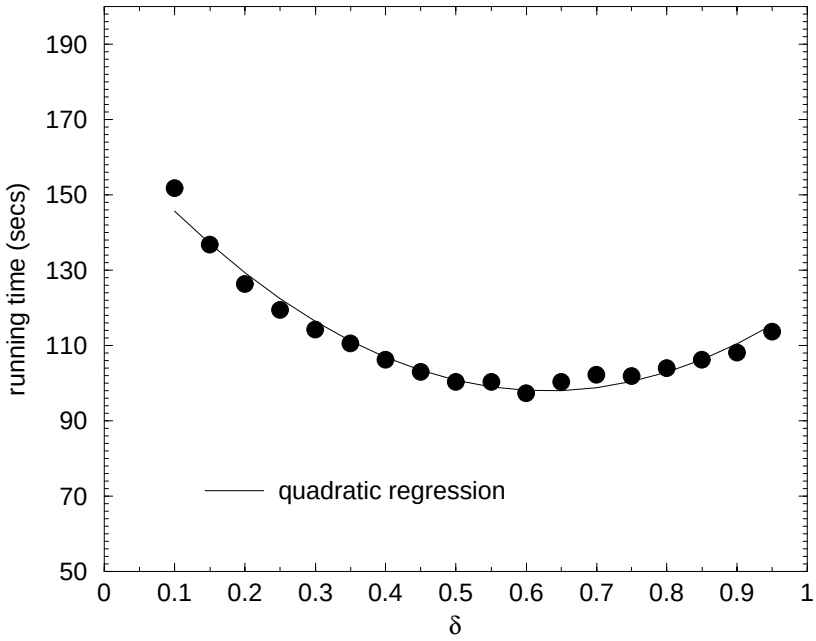

Fig. 5. CPU time required to calculate the effective conductivity of a system of non-overlapping, insulating spherical inclusions dispersed randomly in a conducting matrix with sink volume fraction $\phi_2 = 0.2$. Here, we used the GFFP method with mean diffusion path length $X^2/a^2 = 100$. Times here were measured on a 500 MHz Pentium III work station running Linux over 10^4 Brownian trajectories. This figure shows that an optimal δ is around 0.65.

• important developments in probability theory; these include both the last-passage methods, and methods based on the Feynman-Kac formula [13–15]. Combining all of these methods, allows the treatment of classes of important problems, including the linearized Poisson-Boltzmann equation [16, 17].

This paper is organized as follows: in § 2, we describe the angle-averaging approximations that allow the reduction of a problem based on a vector or tensor Laplace equation, to a problem based on a scalar Laplace equation, *i.e.*, to a diffusion problem. In § 3, we describe the simulation-tabulation (ST) method, that allows extension of the GFFP method to problems in which quasi-analytic Green's functions are not available. In § 4, we discuss the Feynman-Kac method, which allows the use of Monte Carlo diffusion methods to solve a more general class of elliptic boundary value problems. Our emphasis here is on the interaction between the Feynman-Kac methods and the other methods presented here. In § 5, we describe two classes of last-passage algorithms, *i.e.*, Monte Carlo diffusion algorithms in which diffusing particles "initiate" at the point at which they are absorbed, and diffuse "backwards in time." In § 6 we give our conclusions and suggestions for further study.

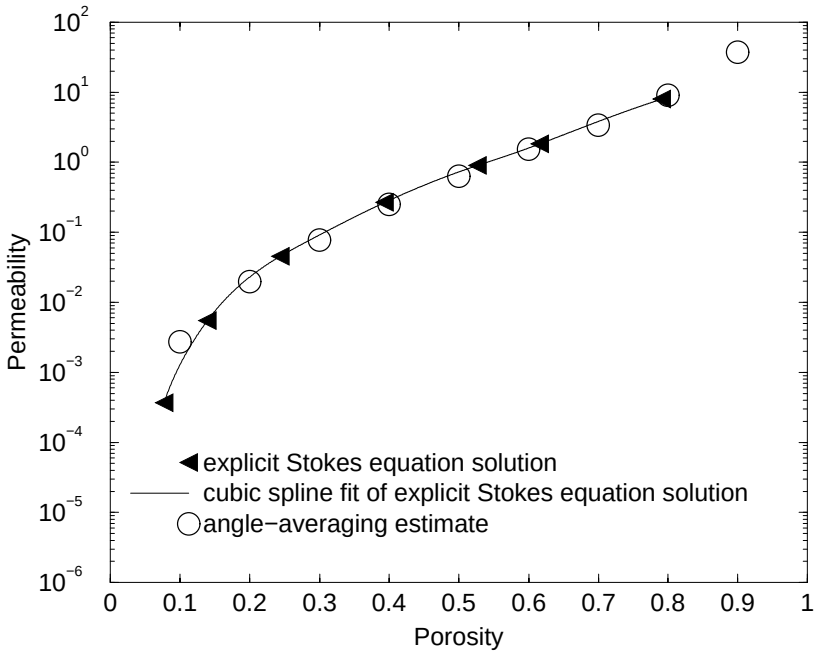

Fig. 6. Permeability, k, versus porosity for a porous medium consisting of a polydispersed mixture of randomly overlapping impermeable spheres. The sphere radii are chosen to have the four values $a = \{1.5, 3.5, 5.5, 7.5\}$ with equal probability.

2 The Angle-Averaging Method

In this section, we describe the angle-averaging method, which allows one to approximate a problem based on a vector or tensor Laplace equation, with a problem based on a scalar Laplace equation. The latter can then be solved using diffusion Monte Carlo methods. The first application of the angle-averaging method was by Hubbard and Douglas [18–20], who gave the following approximation for the translational hydrodynamic friction, f, of an arbitrary object:

$$f = 4\pi\eta C, \tag{1}$$

where η is the fluid viscosity and C the electrical capacitance of an ideal conductor having the same size and shape as the object.

The present authors recently generalized this result to give an algorithm for the permeability of a packed bed, or other porous medium. As an example, in Fig. 6 we present simulation results of packed beds composed of polydispersed overlapping, randomly placed, impenetrable spherical inclusions. The inclusion sphere radii are chosen at random from the values 1.5, 3.5, 5.5, and 7.5 with equal probability. We compare our results with the available numerical solutions of the Stokes equation, [21].

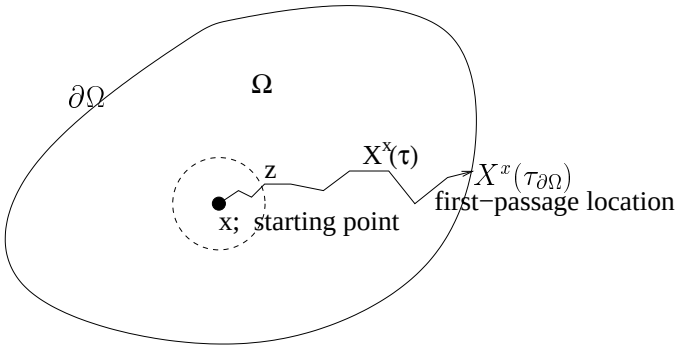

Fig. 7. This figure shows a Brownian motion which starts at $\mathbf{x}$ and terminates at $X^x(\tau_{\partial\Omega})$ on the boundary $\partial\Omega$ while passing through $\mathbf{z}$, a point on a sphere centered at $\mathbf{x}$.

We have also developed an efficient first-passage implementation of this relation. A generalization to the case of a packed bed has direct applications to the properties of suspensions.

The angle-averaging method also provides an approximate relation between the hydrodynamic viscosity of an object and the electrostatic polarizability of an object of the same shape [22, 23].

3 The Simulation-Tabulation (ST) Method

In this section, we explain the ST method, and how to use it to extend the GFFP method to classes of problems for which the Green's function is not available in quasi-analytic form. A basic example is the class of problems involving either mixed or reflecting, *i.e.* Neumann, boundary conditions. This class of problems includes the calculation of the conductivity of a composite medium involving insulating inclusions dispersed in a conducting matrix.

The many-body problem is reduced to the solution of a Laplace or Poisson equation with complicated boundary conditions, *i. e.* it is solved by taking mathematical expectations over Brownian motion trajectories. Since Brownian motion is the microscopic manifestation of diffusion, one can also reinterpret these as diffusion problems [7]. Thus, we need methods to efficiently generate Brownian trajectories in complicated domains. We do this with the help of a useful result from probabilistic potential theory [24, 13]. Namely, we need the fact that the first-passage probability for Brownian motion in a region is *equivalent* to the surface Green's function for the Laplacian in that same region.

While this equivalence is a well-known fact to probabilists and many experts in Monte Carlo, we feel it useful for the rest of our presentation to give an

elementary proof of this fact. First consider the Dirichlet problem for the Laplace equation (see Fig. 7),

$$\Delta u(\mathbf{x}) = 0, \quad \mathbf{x} \in \Omega, \quad u(\mathbf{x}) = f(\mathbf{x}), \quad \mathbf{x} \in \partial\Omega. \tag{2}$$

The solution at point $\mathbf{x}$ can be represented probabilistically as the average over all the boundary values of Brownian motion, $X^{\mathbf{x}}(\tau_{\partial\Omega})$, starting at $\mathbf{x}$ where the Brownian particle first strikes the boundary. The time, $\tau_{\partial\Omega}$, when the Brownian particle first strikes the boundary is called the first-passage time, and the place where the Brownian particle first strikes the boundary, $X^{\mathbf{x}}(\tau_{\partial\Omega})$, is called the first-passage location. Thus we claim that the probabilistic solution, $u_p(\mathbf{x})$, to (2) is given by

$$u_p(\mathbf{x}) = E[f(X^{\mathbf{x}}(\tau_{\partial\Omega}))]. \tag{3}$$

The proof that this is the case is simple. Place a sphere centered at $\mathbf{x}$ completely lying within Ω. Clearly the particle will have to hit this sphere before hitting $\partial\Omega$. The probability distribution of the first-passage location, $\mathbf{z}$, on the sphere is clearly uniform due to the isotropic nature of Brownian motion. Now we continue the Brownian particle from $\mathbf{z}$ until it hits the boundary. Here $X^{\mathbf{x}}(\tau_{\partial\Omega})$ is the first passage location on the boundary, $\partial\Omega$ (see Fig. 7). Averaging over the first-passage boundary values of Brownian paths started at $\mathbf{z}$ gives us $u_p(\mathbf{z})$. Since each trajectory starting at $\mathbf{x}$ that hits $\partial\Omega$ must first hit the sphere with uniform probability, $u_p(\mathbf{x})$ must be the mean of the values of $u_p(\mathbf{z})$ over the sphere. Thus $u_p(\mathbf{x})$ has the mean-value property and is harmonic, *i. e.* it obeys the Laplace equation, [25]. If we then think of moving the starting point for our Brownian particles to the boundary, we clearly will, in the limit, have the first passage location coincide with the limit of $\mathbf{x}$ on the boundary. This argues that, in addition, $u_p(\mathbf{x})$ has the correct boundary values, and so it is the unique solution to (2).

We now use an interpretation of this fact to prove the equivalence mentioned above. Equation (3) can be interpreted as an average of the boundary values, $f(\mathbf{x}), \quad \mathbf{x} \in \partial\Omega$ over $\partial\Omega$. The weighting in this average is the first-passage probability $p(\mathbf{x}, \mathbf{y})$ of a Brownian particle starting at $\mathbf{x}$ hitting the boundary first at $y = X^{\mathbf{x}}(\tau_{\partial\Omega}) \in \partial\Omega$. Thus we can represent $u(\mathbf{x})$ as an integral over the boundary, $\partial\Omega$, via

$$u(\mathbf{x}) = \int_{\partial\Omega} p(\mathbf{x}, \mathbf{y}) f(\mathbf{y}) dy. \tag{4}$$

However, there is another representation of the solution of the Dirichlet problem for the Laplace equation in terms of an integral over the boundary. This is provided by means of the Green's function, $G(\mathbf{x}, \mathbf{y})$, [26]

$$u(\mathbf{x}) = \int_{\partial\Omega} \frac{\partial G(\mathbf{x}, \mathbf{y})}{\partial \mathbf{n}} f(\mathbf{y}) dy. \tag{5}$$

The normal derivative of the Green's function on $\partial\Omega$ is what we refer to as the "surface Green's function" for the domain Ω. Thus the surface Green's function for a domain, Ω, must be *equivalent* to the first-passage probability distribution

for that same domain: $p(\mathbf{x}, \mathbf{y}) = \partial G(\mathbf{x}, \mathbf{y})/\partial \mathbf{n}$. With this fact, our strategy becomes the use of surface Green's functions to act as probability distributions to move Brownian particles quickly through their trajectories while maintaining their exact distribution properties.

The ST method greatly extends the GFFP method by allowing its application to domains for which we have no analytic representation of the Green's function. Perhaps the most basic example is the escape of a diffusing particle from a reflecting, *i.e.*, non-absorbing sphere. This is important as many FP domains involving either reflecting, or mixed, boundary conditions provide examples of this type.

The ST method is implemented as follows: for each set of values of the geometric parameters that characterize a particular FP surface, one performs a large number of simulations. For each simulation, the FP position is noted and the dimensionless parameters that characterize it are binned. The normed average of these binned values is partially integrated to give the distribution function for first-passage. This quantity is then tabulated, and a high-precision interpolatory fit is applied to it. This procedure, though numerically intensive, need only be carried out once for each FP geometry. The result, a tiny dataset consisting of the values of the resulting interpolation parameters, can then be used, rapidly and efficiently, to sample the FP position for this absorbing FP surface. This is a bootstrap methodology: the simulation phase of an initial ST application uses only WOS; subsequent applications are more efficient because each uses the results of the previous ST tabulations.

The ST method can be used to sample the FP position, *i.e.*, the absorption position, for Dirichlet Laplace problems in which the FP surface can be characterized by either one or two dimensionless parameters. This last limitation is purely computational; a tabulation of a problem of this kind that uses three parameters will be a natural supercomputer project once it is motivated.

The ST method has been applied to calculate the electrical conductivity of a composite material composed of non-overlapping, non-conducting spherical inclusions randomly dispersed in a conducting matrix. This is a specific case of a problem first studied in detail by Kim and Torquato. Our results (see Figs. 3- 5) agree with theirs in detail, although our computation times are shorter.

Second, the ST method is not limited to obtaining the FP position of a diffusing particle. Calculations of electrical conductivity require knowledge of the FP time. But any quantity may be sampled using the ST method. For example, the Feynman-Kac formulation of the linearized Poisson-Boltzmann equation requires sampling the exponential of the FP time. We discuss this next.

4 The Feynman-Kac Method

In this section, we explain the Feynman-Kac method for solving the Schrödinger equation, and other elliptic partial differential equations. We discuss the interaction between this method and methods already detailed in this review.

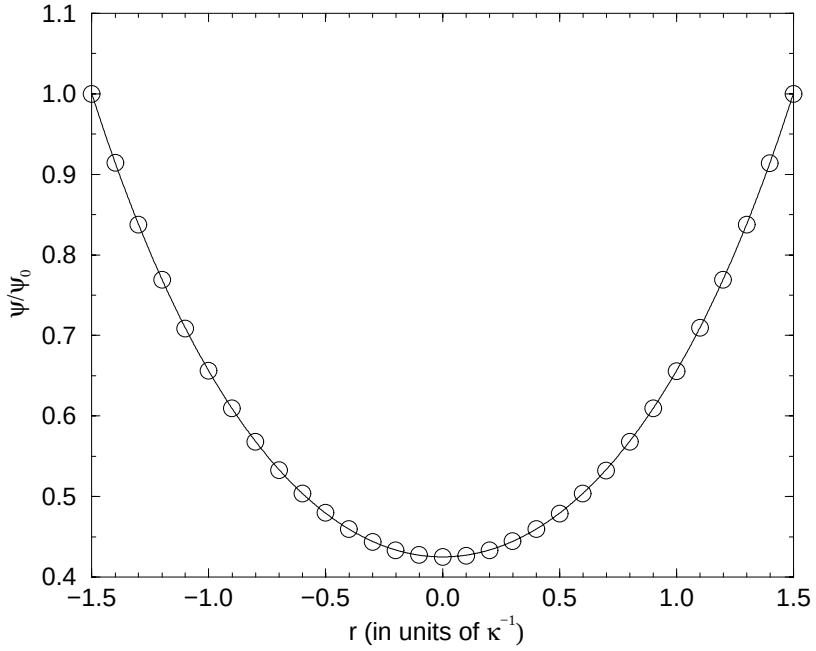

Fig. 8. The electric potential in an electrolyte between two infinite charged parallel flat plates. The solid line is the analytic solution and the circles are the simulation results with 10^6 random walks using an absorption layer thickness of $\delta = 10^{-4}$. Here, r is the distance from the mid-point of the plates and κ the inverse Debye length.

The Feynman-Kac formulation of the Dirichlet problem for the classical Schrödinger equation:

$$\frac{1}{2}\Delta\phi + V(x)\phi = 0, \qquad \mathbf{x} \in \Omega \tag{6}$$

$$\phi(\mathbf{x}) = \Psi(\mathbf{x}), \qquad \mathbf{x} \in \partial\Omega \tag{7}$$

provides a formula for the value of the field ϕ at a point x, namely [13,14]:

$$\phi(\mathbf{x}) = E[\Psi(X(\tau_{\partial\Omega}))\exp\{\int_0^{\tau_{\partial\Omega}} V(X(\tau_{\partial\Omega}))d\tau\}]. \tag{8}$$

where $\tau_{\partial\Omega} = \{\tau : X(\tau) \in \partial\Omega\}$ is the FP time and $X(\tau_{\partial\Omega})$ is the FP point of X, the Brownian motion started at $\mathbf{x}$.

An elementary example of the Schrödinger equation, but one of extensive importance in molecular biology, is the linearized Poisson-Boltzmann equation [16]:

$$\Delta\phi - \kappa^2\phi = 0, \qquad \mathbf{x} \in \Omega \tag{9}$$

$$\phi(\mathbf{x}) = \Psi(\mathbf{x}), \qquad \mathbf{x} \in \partial\Omega \tag{10}$$

Here ϕ gives the electrical potential in the neighborhood of a biomolecule immersed in an electrolyte; κ is the Debye constant of the electrolyte. The Feynman-Kac formulation, applied to this problem, gives the formula for ϕ:

$$\phi(\mathbf{x}) = E[\Psi(X(\tau_{\partial\Omega}))\exp\{-\int_0^{\tau_{\partial\Omega}} \kappa^2 d\tau\}], \tag{11}$$

where $\tau_{\partial\Omega} = \{\tau : X(\tau) \in \partial\Omega\}$ is the FP time and $X(\tau_{\partial\Omega})$ is the FP point. For a spherical FP surface, the κ^2-term, interpreted as a standard decay rate, produces the decimation probability [27, 17]:

$$E[\exp(-\kappa^2 t)] = \frac{d\kappa}{\sinh d\kappa}, \tag{12}$$

Here d is the FP sphere radius. The FK formulation given above reproduces the formula. But, it is much more general. For a more complicated FP surface, the LHS of the above equation can still be determined, using the ST method, even though analytic results are no longer available. Using the entire first-passage time probability distribution, we illustrate its computational equivalence to the decimation probability via the parallel plates problem used in previous research [16, 17]. The results are given in Fig. 8.

5 Last Passage Methods for Diffusion Monte Carlo

In this section, we develop the concept of last-passage diffusion and explain its importance to the realm of Monte Carlo diffusion problems. Because this concept will be novel to most readers of this review, we will explain both the motivations for the concept and its two rather different realizations in practice.

The methodology for solving diffusion Monte Carlo problems that we have described in previous sections of this review is optimal for a large class of problems in which diffusing particles initiate outside a complex material domain and terminate on portions of its surface.

It is a fact, well known in pure mathematics, but apparently not in the realm of applied mathematics, that many diffusion Monte Carlo problems can be adequately described by using both 'first-passage diffusion', and also 'last-passage diffusion' methods [6]. The latter involves diffusing particles that initiate on or near their absorption points, and diffuse "backwards in time." Here we develop the first of two basic last-passage algorithms: the external-origin last-passage (EOLP) algorithms. These were developed by our group.

The charge density $\sigma(x)$ at a point, x, on the surface of an absorbing object is given by the equation:

$$\sigma(x) = \frac{1}{4\pi}\int_{y\in\partial\Omega_x} d^2y G(x,y) P_{y\to\infty}. \tag{13}$$

Here the surface, $\partial\Omega_x$, is that part of a sphere with x as center, that is, outside the absorbing surface and the factor $P_{y\to\infty}$ is the probability that a diffusing

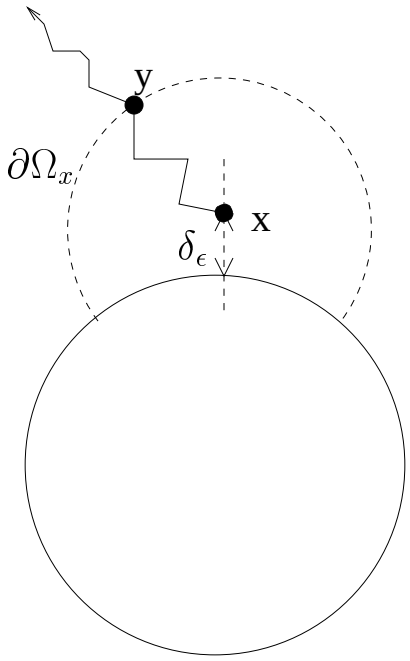

Fig. 9. The voltage $V(x)$ near a conducting sphere, at the point x, is given in diffusion language by the probability that a diffusing particle starting at point x will diffuse away to infinity without hitting the sphere. In order to do so, it must first reach a FP surface, $\partial\Omega_x$, drawn around point x and then proceed to diffuse far away without returning.

particle, initiating at point $y \in \partial\Omega_x$, diffuses to infinity without returning to the absorbing surface. The function $G(x, y)$ is defined by:

$$G(x, y) = \frac{d}{d\delta_\epsilon}\bigg|_{\delta_\epsilon = 0} g(x, y). \tag{14}$$

Here $g(x, y)$ is the Laplace Green's function on the surface, $\partial\Omega_x$ with source point x at a distance δ_ϵ from the absorbing surface.

To derive Eq. 13, first consider the function $V(x)$ that gives the probability that a diffusing particle initiating at a point x near to the surface of an absorbing object, touches, *i.e.* makes first passage at the surface of the object in finite time (see Fig. 9). This is a harmonic function; it is unity on the surface of the object, and zero at infinity. Thus, by uniqueness of solutions to the Laplace equation, it is identical to the voltage surrounding the object when it is at voltage unity

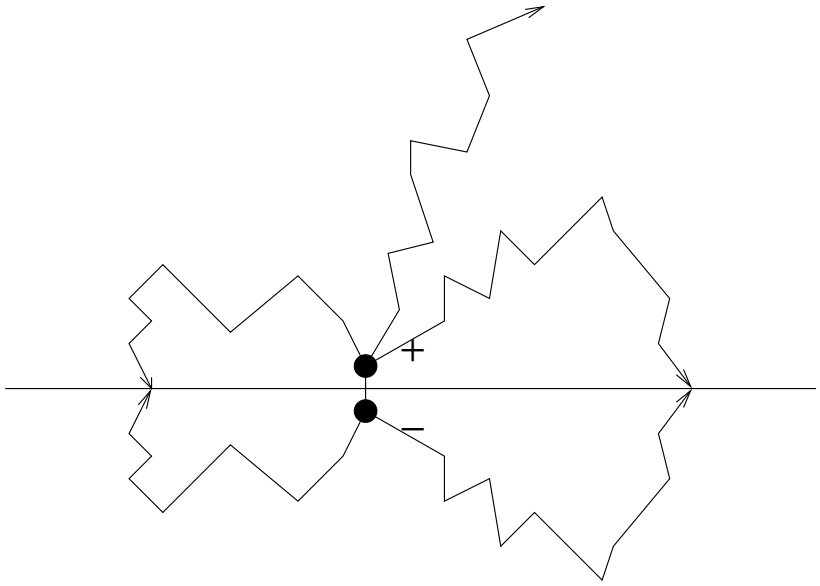

Fig. 10. The Green's function for a point dipole oriented normal to an absorbing surface is a generating function for diffusing particle trajectories that leave the absorbing surface and never return. The effect of trajectories that leave and do return is zero; they cancel out in pairs.

with respect to infinity. By the Gauss theorem, the charge density, $\sigma(x)$, at a point on the surface is given by

$$\sigma(x) = -\frac{1}{4\pi}\frac{d}{d\delta_\epsilon}\bigg|_{\delta_\epsilon=0} V(x). \tag{15}$$

Representing $V(x)$ as in Fig. 9, and realizing that only the δ_ϵ-dependence of the probability density for the first step is relevant (because it is proportional to δ_ϵ), gives Eq. 13.

The function $G(x, y)$ is a point-dipole Green's function. To see this, note that taking the δ_ϵ-derivative and setting δ_ϵ to zero in Eq. 15 has the same effect as taking the dipole limit: allowing both the magnitude Q of the source at point x, and that of its image charge, to grow without limit as $\delta_\epsilon \to 0$, while keeping the quantity $Q^2\delta_\epsilon$ finite. Placing a point dipole at point x provides a source for all of the diffusing particle trajectories that originate at the point x leave and never return. The probability of escape from an absorbing surface is rigorously zero; this Green's function samples only the measure-zero subset of trajectories that succeed. Fig. 10 shows a simple case in which this claim can be easily verified by inspection. This formula (and this Green's function) were developed to provide a local formula for charge density, *i.e.*, a formula that could be used regardless of other nearby charges and conductors.

Both the calculation of the capacitance of a non-smooth object and the two other classes of problems mentioned above can also be treated with the other class of last-passage methods, the integral-origin last-passage (IOLP) methods. The equilibrium charge distribution $\sigma(x)$ on an absorbing object is given by:

$$\sigma(x) = 2\pi|x - z|L(x, z), \tag{16}$$

where $L(x, z)$ is the last passage distribution. Here diffusing particles initiate at a point z interior to an absorbing object. They diffuse, ignoring the absorbing object, until they eventually diffuse away to infinity. At this time, the point, x, of last contact, *i.e.*, last-passage, with the absorbing object is determined. We do this using a generalization of the dipole Green's function defined in Eq. 14; this is detailed in a forthcoming publication.

None can yet describe the relative advantages of these two sets of last-passage methods; this research is now in progress.

There are at least three classes of diffusion Monte Carlo problems for which last-passage algorithms are optimal:

• Charge distribution on a conducting object with edges and corners. In such problems, a large fraction of the charge will collect very close to the edges and corners, *i.e.*, on a very small subset that is readily identified in advance. Thus last-passage algorithms are appropriate.

• Problems in which a large fraction of the absorption takes place on a very small fraction of the surface, because of the imposed boundary conditions. The basic example here is the problem of diffusion-limited absorption of a ligand molecule at a small absorbing site on a macromolecule. If the absorbing site is small enough, it must become optimal computationally for the diffusing particles to initiate on the absorbing site rather than to initiate on an external launch sphere and 'search for' the absorbing site. The Solc-Stockmayer model of protein-ligand binding is perhaps the best-studied model of this process [12, 28].

• Problems in which more than one conducting object is present, at close proximity, and at different voltages. In these cases (modern micro-electronics provides many examples), one seeks to calculate not a capacitance but an entire capacitance matrix. Here, no launch surface for diffusing particles can be defined; so first passage algorithms are not a possibility.

We will discuss examples of the first class of applications; examples of the two other classes will be published separately.

A basic well-studied example of the first class is that of a conducting cube. If first-passage methods are used to study this problem, importance sampling will occur, *i.e.*, the correct surface charge distribution will be obtained only if a large launch sphere is used. This will not be optimal in a computational sense. optimality in a computational sense. In the last-passage algorithm, the capacitance of the unit cube is defined to be the integral, over the surface of the cube of the surface charge density $\sigma(x)$ as given by Eq. 19; it is defined as a double integral. Importance sampling is readily imposed on the outside integral, *i.e.*, the integral over σ by using the measure:

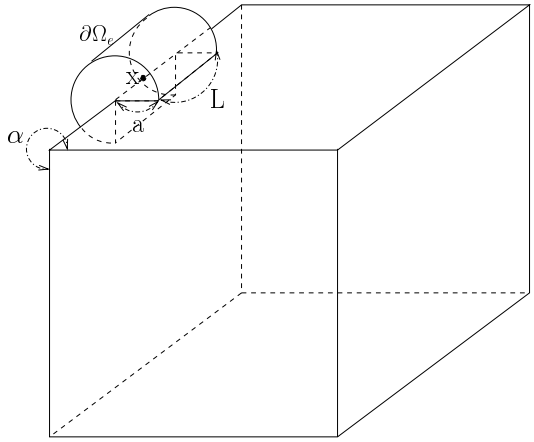

Fig. 11. A three-quarter cylinder of radius a and length L on the edge of a cube is shown.

$$x = (1 - \eta^{3/2}). \tag{17}$$

$$y = (1 - \eta^{3/2}). \tag{18}$$

Here, (x, y) is the sampling point on the sampling area, $(0, 1) \times (0, 1)$, in x-y plane and the η's are independent random numbers uniformly distributed in $(0, 1)$. If this measure is used, almost all points at which the charge density must be sampled will be close to the edge of the cube. The statistics of the inner integral, *i.e.*, the integral that gives $\sigma(x)$, will be very poor because the probability $P_{y\to\infty}$ will be very close to zero. An important method of overcoming this problem is the method of the edge distribution.

For any edge on a conducting surface the charge distribution $\sigma(x, \delta_e)$ on a curve parallel to the edge, but separated from it by distance δ_e, with δ_e small, is given by:

$$\sigma(x, \delta_e) = \delta_e^{\pi/\alpha - 1} \sigma_e(x). \tag{19}$$

Here $\sigma_e(x)$ is what we term the edge distribution. α is the angle between the two intersecting surfaces, here $\alpha = 3\pi/2$. The edge distribution has a natural probabilistic interpretation: it is the (rescaled) probability density that a diffusing particle makes last passage on the edge point x. This distribution can be calculated either by simulation (see Fig. 10) or by application of the general formula from Eq. 19. The point is that this one-dimensional distribution need be calculated only once for each edge on each absorbing object in a problem. An

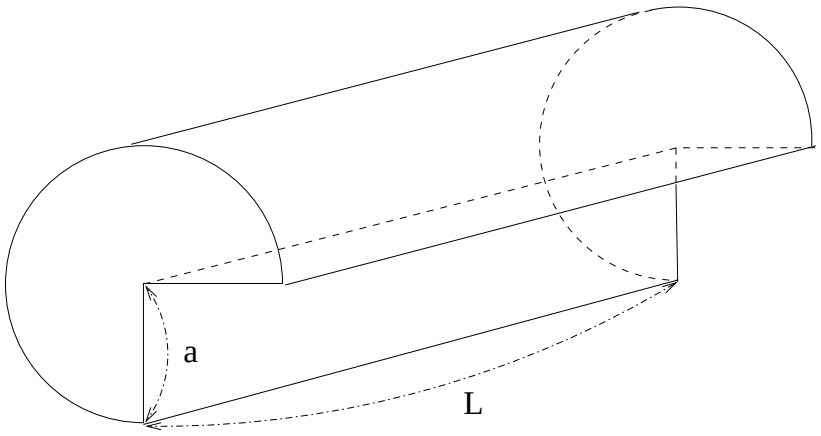

Fig. 12. A three-quarter cylinder of radius a and length L is shown.

extension of Eq. 13 for $\sigma(x)$ gives a formula for the edge distribution:

$$\sigma_e(x) = \frac{1}{4\pi} \lim_{\delta_e \to 0} \delta_e^{1-\pi/\alpha} \int_{y \in \partial\Omega_e} d^2y G(x,y) P_{y\to\infty}. \tag{20}$$

Here $\partial\Omega_e$ is a cylindrical surface that intersects the pair of absorbing surfaces meeting at angle α (see Fig. 11). The other quantities have already been defined.

For the function $G(x,y)$, we start with the potential inside a grounded cylindrical box defined by the surfaces $z = 0$, $z = L$, and $\rho = a$ with a unit point charge located at the point (ρ', ϕ', z') given by [29]:

$$\Phi(\rho,\phi,z) = \frac{4}{L} \sum_{m=-\infty}^{\infty} \sum_{n=1}^{\infty} e^{im(\phi-\phi')} \sin\Big(\frac{n\pi z}{L}\Big) \sin\Big(\frac{n\pi z'}{L}\Big) \frac{I_m(\frac{n\pi\rho_<}{L})}{I_m(\frac{n\pi a}{L})} \times \Big[I_m\Big(\frac{n\pi a}{L}\Big) K_m\Big(\frac{n\pi\rho_>}{L}\Big) - K_m\Big(\frac{n\pi a}{L}\Big) I_m\Big(\frac{n\pi\rho_>}{L}\Big)\Big]. \tag{21}$$

Here, I_m and K_m are modified Bessel functions and

$$\rho_< = \min(\rho', \rho), \tag{22}$$

$$\rho_> = \max(\rho', \rho). \tag{23}$$

Modifying Eq. 21 to satisfy the boundary conditions of a three-quarter cylinder (see Fig. 12), the potential inside the three-quarter cylinder when $\rho' < \rho$ is obtained as

$$\Phi_c(\rho,\phi,z) = \frac{4}{L} \sum_{n=1}^{\infty} \sin\Big(\frac{2}{3}\phi\Big) \sin\Big(\frac{2}{3}\phi'\Big) \sin\Big(\frac{n\pi z}{L}\Big) \sin\Big(\frac{n\pi z'}{L}\Big) \frac{I_{2/3}(\frac{n\pi\rho'}{L})}{I_{2/3}(\frac{n\pi a}{L})} \times \Big[I_{2/3}\Big(\frac{n\pi a}{L}\Big) K_{2/3}\Big(\frac{n\pi\rho}{L}\Big) - K_{2/3}\Big(\frac{n\pi a}{L}\Big) I_{2/3}\Big(\frac{n\pi\rho}{L}\Big)\Big]. \tag{24}$$

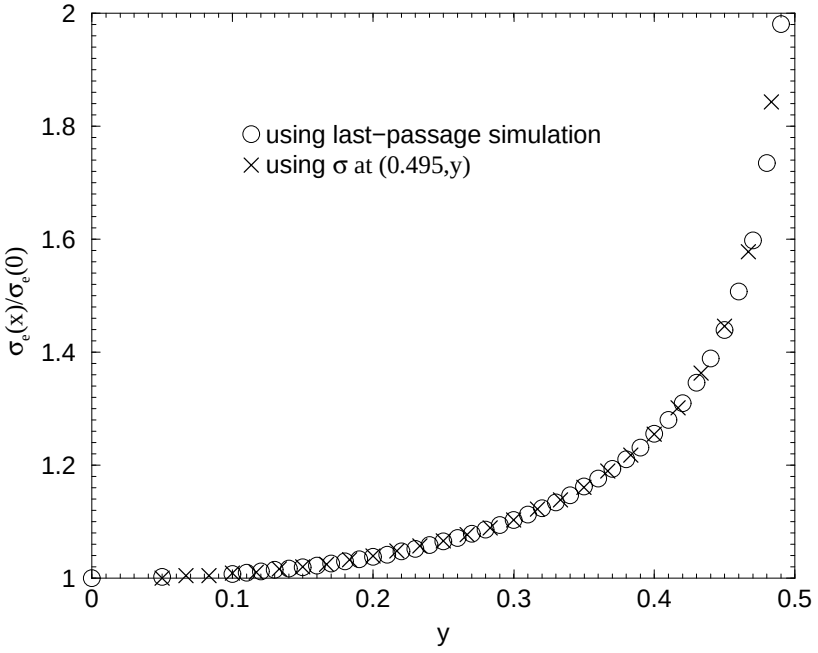

Fig. 13. The edge distribution of a unit cube calculated using Eq. 19 and using Eq. 20.

Hence, $G(\phi,z)_{\rho=a}$ for the side of the three-quarter cylinder is given by

$$G(\phi,z)_{\rho=a} = \frac{1}{\Gamma(5/3)2^{2/3}}\frac{4}{9\pi La}\sum_{n=1}^{\infty}\sin\Big(\frac{2}{3}\phi\Big)\sin\Big(\frac{n\pi z}{L}\Big)\sin\Big(\frac{n\pi z'}{L}\Big) \times\Big(\frac{n\pi}{L}\Big)^{2/3}\frac{1}{I_{2/3}(\frac{n\pi a}{L})} \qquad (25)$$

and $G(\rho,\phi)_{z=0}$ for the lower cap of the three-quarter cylinder

$$G(\rho,\phi)_{z=0} = \frac{1}{\Gamma(5/3)2^{2/3}}\frac{4}{9\pi L}\sum_{n=1}^{\infty}\sin\Big(\frac{2}{3}\phi\Big)\Big(\frac{n\pi}{L}\Big)^{5/3}\sin\Big(\frac{n\pi z'}{L}\Big) \times\frac{1}{I_{2/3}(\frac{n\pi a}{L})}\Big[I_{2/3}\Big(\frac{n\pi a}{L}\Big)K_{2/3}\Big(\frac{n\pi\rho}{L}\Big) - K_{2/3}\Big(\frac{n\pi a}{L}\Big)I_{2/3}\Big(\frac{n\pi\rho}{L}\Big)\Big]. \qquad (26)$$

Thus the edge distribution of a cube (see Fig. 13), $\sigma_e(x)$ is obtained as

$$\sigma_e(x) = 2\int_0^a\int_0^{3\pi/2} G(\rho,\phi)_{z=0}P_{y\to\infty}\rho d\phi d\rho + a\int_0^L\int_0^{3\pi/2} G(\phi,z)_{\rho=a}P_{y\to\infty}d\phi dz, \qquad (27)$$

where $P_{y\to\infty}$ is the probability of going to infinity from the point y on the side or caps of the chopped cylinder.

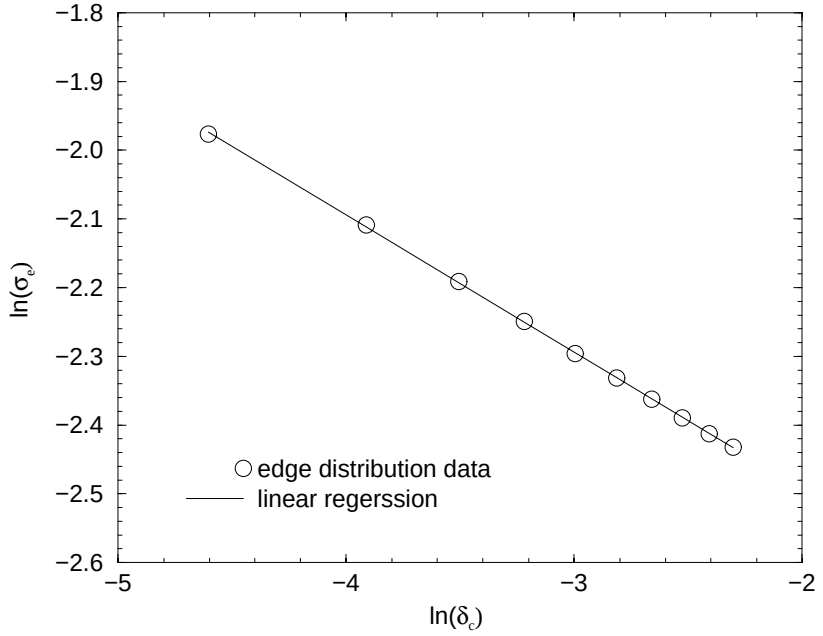

Fig. 14. Asymptotic values near the corner of the edge distribution for a unit cube: δ_c is the distance from the corner and the slope is approximately -0.20.

For convenience, a chopped cylinder of $L = a = 0.02$ is used and the edge calculations are done at the center of the chopped cylinder on a unit cube moving the chopped cylinder along the edge of the cube (see Fig. 11). Due to the symmetry of the cube, the edge distribution is obtained in the range of $(0, 0.49)$ with 0.01 step. The result is shown in Fig. 13. However, because the charge singularity at a corner is stronger that that at an edge, the edge distribution near the corner diverges. To use the edge distribution for the fast calculation of the capacitance of a cube, we calculate the asymptotic behavior near the corner. The exponent of the edge distribution near the corner is approximately -0.20, that is, $\sigma_e \sim \delta_c^{-1/5}$ (see Fig. 14).

The edge distribution can be calculated for a conducting object, provided it consists of a segment of a line or an arc of a circle, using generalizations of the methods discussed here. These distributions can then be used to calculate the surface charge density on the conducting object using a rapid importance sampling algorithm. Such algorithms are rapid because they tell us in advance the detailed charge distribution near edges and corners.

We believe that this last passage method is the fastest method to date for solving this basic set of problems. Computing the capacitance of a cube has been considered to be "one of the major unsolved problems of electrostatic theory," [20].

6 Conclusions and Suggestions for further study

In this paper, we review the results so far obtained from applying the set of Monte Carlo diffusion methods we have developed and assembled. The results already exhibited demonstrate that a number of classes of important problems can be solved far more efficiently using these methods.

The potential of this class of methods is yet to be tapped. Here we note just two examples of important extensions:

• Solution of the linearized Poisson-Boltzmann equation in general requires solution of problems with dielectric boundaries, *i.e.*, nontrivial values of the dielectric constant on both sides of the interface. Green's functions for this purpose are available; they can be tabulated.

• Calculation of the mutual capacitance matrix for a system of conductors in close proximity. Last passage methods allow calculation of this quantity using diffusion Monte Carlo. It remains to be seen which of these methods most efficient.

ACKNOWLEDGMENTS

We give special thanks to John David Jackson, Joe Hubbard, Kai Lai Chung, Karl K. Sabelfeld, and Henry P. McKean for their useful discussions.

References

1. A. Haji-Sheikh and E. M. Sparrow. The solution of heat conduction problems by probability methods. *Journal of Heat Transfer*, 89:121–131, 1967.
2. I. C. Kim and S. Torquato. Effective conductivity of suspensions of hard spheres by Brownian motion simulation. *J. Appl. Phys.*, 69(4):2280–2289, 1991.
3. I. C. Kim and S. Torquato. Effective conductivity of suspensions of overlapping spheres. *J. Appl. Phys.*, 71(6):2727–2735, 1992.
4. S. Torquato, I.-C. Kim, and D. Cule. Effective conductivity, dielectric constant, and diffusion coefficient of digitized composite media via first-passage-time equations. *J. Appl. Phys.*, 85:1560–1571, 1999.
5. C.-O. Hwang, J. A. Given, and M. Mascagni. On the rapid calculation of permeability for porous media using Brownian motion paths. *Phys. Fluids A*, 12(7):1699–1709, 2000.
6. K. L. Chung. *Green, Brown, and Probability.* World Scientific, Singapore, 1995.
7. J. A. Given, J. B. Hubbard, and J. F. Douglas. A first-passage algorithm for the hydrodynamic friction and diffusion-limited reaction rate of macromolecules. *J. Chem. Phys.*, 106(9):3721–3771, 1997.
8. M. E. Müller. Some continuous Monte Carlo methods for the Dirichlet problem. *Ann. Math. Stat.*, 27:569–589, 1956.
9. T. E. Booth. Exact Monte Carlo solution of elliptic partial differential equations. *J. Comput. Phys.*, 39:396–404, 1981.
10. S. Torquato and I. C. Kim. Efficient simulation technique to compute effective properties of heterogeneous media. *Appl. Phys. Lett.*, 55:1847–1849, 1989.
11. C.-O. Hwang, J. A. Given, and M. Mascagni. Rapid diffusion Monte Carlo algorithms for fluid dynamic permeability. *Monte Carlo Methods and Applications*, 7(3-4):213–222, 2001.

12. C.-O. Hwang, J. A. Given, and M. Mascagni. The simulation-tabulation method for classical diffusion Monte Carlo. *J. Comput. Phys.*, submitted, 2000.
13. M. Freidlin. *Functional Integration and Partial Differential Equations.* Princeton University Press, Princeton, New Jersey, 1985.
14. K. L. Chung and Z. Zhao. *From Brownian Motion to Schrödinger's Equation.* Springer-Verlag, Berlin, 1995.
15. K. K. Sabelfeld. Integral and probabilistic representations for systems of elliptic equations. *Mathematical and Computer Modelling*, 23:111–129, 1996.
16. R. Ettelaie. Solutions of the linearized Poisson-Boltzmann equation through the use of random walk simulation method. *J. Chem. Phys.*, 103(9):3657–3667, 1995.
17. C.-O. Hwang and M. Mascagni. Efficient modified "Walk On Spheres" algorithm for the linearized Poisson-Boltzmann equation. *Appl. Phys. Lett.*, 78(6):787–789, 2001.
18. J. B. Hubbard and J. F. Douglas. Hydrodynamic friction of arbitrarily shaped Brownian particles. *Phys. Rev. E*, 47:R2983–R2986, 1993.
19. J. F. Douglas, H.-X. Zhou, and J. B. Hubbard. Hydrodynamic friction and the capacitance of arbitrarily shaped objects. *Phys. Rev. E*, 49:5319–5331, 1994.
20. H.-X. Zhou, A. Szabo, J. F. Douglas, and J. B. Hubbard. A Brownian dynamics algorithm for caculating the hydrodynamic friction and the electrostatic capacitance of an arbitrarily shaped object. *J. Chem. Phys.*, 100(5):3821–3826, 1994.
21. N. S. Martys, S. Torquato, and D. P. Bentz. Universal scaling of fluid permeability for sphere packings. *Phys. Rev. E*, 50:403–408, 1994.
22. H.-X. Zhou. Calculation of translational friction and intrinsic viscosity. I. General formulation for arbitrarily shaped particles. *Biophys. J.*, 69:2286–2297, 1995.
23. H.-X. Zhou. Calculation of translational friction and intrinsic viscosity. ii. application to globular proteins. *Biophys. J.*, 69:2298–2303, 1995.
24. S. C. Port and C. J. Stone. *Brownian Motion and Classical Potential Theory.* Academic Press, New York, 1978.
25. F. John. *Partial Differential Equations.* Springer-Verlag, Berlin, Heidelberg, and New York, 1982.
26. E. C. Zachmanoglou and D. W. Thoe. *Introduction to Partial Differential Equations with Applications.* Dover, New York, 1976.
27. B. S. Elepov and G. A. Mihailov. The "Walk On Spheres" algorithm for the equation $\delta u - cu = -g$. *Soviet Math. Dokl.*, 14:1276–1280, 1973.
28. H.-X. Zhou. Comparison of three Brownian-dynamics algorithms for calculating rate constants of diffusion-influenced reactions. *J. Chem. Phys.*, 108(19):8139–8145, 1998.
29. J. D. Jackson. *Classical Electrodynamics.* John Wiley and Sons, Inc., New York, 1975.